Dynamics of end-tethered chains at high surface coverage

Yogesh M. Joshi[a)]

Chemical Engineering Division, National Chemical Laboratory, Pune, 411 008, India

Ashish K. Lele[b)]

Department of Chemical Engineering, University of Cambridge, Pembroke Street, Cambridge CB2 3RA, UK

(Received 29 June 2001; final revision received 20 November 2001)

Synopsis

A molecular model for wall slip [Y. M. Joshi *et al.*, Macromolecules **34**, 3412 (2001)] based on recent tube theories is extended to account for the effects of entanglements between tethered chains that occur at higher surface coverage. Three regimes of surface coverage are identified. Regime I is a low surface coverage regime (the mushroom regime), which has been discussed earlier by us. In regime II the tethered chains undergo a cooperative constraint release process due to which the slip velocity increases with surface coverage while the slip length becomes independent of the surface coverage. In regime III the tethered chains start to become entangled with each other thereby causing the interfacial modulus, the critical wall shear stress and the critical shear rate to decrease with surface coverage. Our model is different from previous scaling models in that it provides a constitutive equation for tethered chains. As a result, it offers scope for quantitative prediction of microscopic and macroscopic experimental slip data based solely on molecular information. Our model also predicts scaling laws for the various slip parameters in the three regimes of surface coverage. These laws are in general agreement with previously reported scaling models and experimental data. © *2002 The Society of Rheology.* [DOI: 10.1122/1.1446880]

I. INTRODUCTION

The topic of extrusion instabilities has been investigated for more than five decades and the large body of work has been reviewed several times [see, for example, Work of Denn (2001) and of Wang (1999)]. We have been interested in understanding the role of tethered chain dynamics on the interfacial stick–slip instability [Joshi *et al.* (2000a, 2000b)]. It is now generally accepted that for a strongly adsorbing wall sudden slip occurs by a disentanglement mechanism, which was formalized into a scaling model by Brochard and de Gennes (1992). We have recently proposed a tube model for the dynamics of end-tethered chains that are sparsely grafted on a strongly adhesive wall [Joshi *et al.* (2001); Joshi (2001)]. In this article we are concerned with further development of

[a)]Current address: The Levich Institute, City College of the City University of New York, 140th Street at Convent Avenue, New York, NY 10031.

[b)]Author to whom correspondence should be addressed; electronic mail: lele@che.ncl.res.in. Permanent address: Chemical Engineering Division, National Chemical Laboratory, Pune, 411 008, India.

the tube model for regimes of higher surface coverage including the one in which different tethered chains start becoming entangled with each other.

The disentanglement model of Brochard and de Gennes (1992) considers the flow of a polymer melt along a wall on which the chains of the same polymer are end tethered and are entangled with the flowing bulk chains. The model was developed for the case of low grafting density of tethered chains (the so-called ''mushroom'' region), in which different tethered chains do not overlap. Brochard and de Gennes (1992) argued that under the influence of flow a tethered polymer chain deforms into a ''cigar'' shaped coil. When the diameter of the deforming cylindrical coil of a tethered molecule decreases below the entanglement spacing, the bulk chains suddenly become disentangled from the tethered chains causing discontinuous slip.

Ajdari *et al.* (1994) considered the case of a probe chain being pulled by its end through a stationary bulk. This situation is equivalent to the case of bulk chains flowing past a stationary wall grafted with an end-tethered chain. Adjari *et al.* (1994) recognized that the probe chain relaxes its stress in a manner similar to that of an arm of a star polymer. Whereas usual reptational diffusion is not possible because of tethering at one end, the modes of relaxation available to the probe chain are arm retraction and constraint release. Mhetar and Archer (1998) also considered the problem of pulling a probe chain through entangled stationary bulk chains but proposed a different approach for calculating the friction on the probe chain. They estimated the friction coefficient by considering the local conformations of the deforming probe chain, which could be classified as ball, ball–cylinder and ball–cylinder–stick conformations, respectively, at increasing pulling speeds. Various scaling laws were predicted from this analysis and they agreed well with various experimental predictions.

Macroscopic controlled-stress capillary extrusion experiments have provided an indirect validation of the disentanglement hypothesis. Specifically, Wang and Drda (1996) showed that the critical stress for discontinuous slip scaled linearly with the temperature as expected from the disentanglement model. Direct comparison with the disentanglement model was achieved by Leger and co-workers [Leger *et al.* (1996b); Leger *et al.* (1997); Leger *et al.* (1999)] who used an evanescent wave near field velocimetry (NFV) technique to determine of the velocity of polymer molecules up to 70–100 nm near the wall. This distance was within a few (at least three) radii of gyration of the bulk chains and thus provided a direct microscopic means of measuring the slip velocity close to the wall. A polydimethylsiloxane (PDMS) melt of different molecular weights was sheared between two surfaces of silica separated by a few microns by moving the top plate with controlled velocity. The slip velocity was measured by the NFV technique. In some experiments, the silica surfaces were tailored to produce grafted layers of end-tethered chains at various surface coverages. Three friction regimes were observed. In the first regime, the slip length was found to be independent of the slip velocity. In the second regime, which started above a critical velocity, the slip length increased with a power law dependence on the slip velocity. In the third regime, the slip length again became independent of the slip velocity and the magnitude of b was found to be several orders of magnitude higher than the molecular dimensions [Leger *et al.* (1996b, 1999)]. These observations validated the qualitative features of the scaling model of Brochard and de Gennes (1992).

The scaling model for sudden disentanglement inherently assumes that a tethered chain is able to orient more easily under shear compared to bulk chains. We have recently proposed a molecular explanation of this phenomenon [Joshi *et al.* (2001)]. Specifically, we showed that the tethered chain experiences suppressed convective constraint release relaxation, which is unable to randomize its orientation caused by the flowing bulk

chains. Our model was based on the contour variable (CV) tube model [Mead *et al.* (1998)] and is different from the previous scaling models in that it proposes a constitutive equation for the dynamics of end-tethered chains. The scaling laws for the molecular weight dependence of the slip parameters can be easily derived from the constitutive equation and are in agreement with the previous scaling models. More important, our model has the capability to quantitatively predict slip parameters based only on molecular information.

Our tube model was restricted to sparsely grafted walls, whereas in a real extrusion process the chains close to the die walls could adsorb and form an interfacial layer of high grafting density. Thus, it is essential to understand the effects of the grafting density on slip parameters. Durliat *et al.* (1997) carried out experiments for different surface coverages and observed that the critical shear rate shows a maximum with respect to the grafting density. They inferred that the critical shear rate increases initially because of the additive effect of friction from each of the independent tethered chains, whereas at high surface coverage, the critical shear rate decreases because of the collective behavior of the tethered chains. They also found that the slip length was independent of the molecular weight of bulk and the surface coverage. Brochard-Wyart *et al.* (1996) proposed a scaling model for the grafting density that was higher than in the mushroom regime but lower than in the overlap regime. They showed that above a threshold surface coverage when all the bulk chains near the wall are trapped, the low velocity friction becomes independent of the surface coverage. As a result, the critical slip velocity increases linearly with the surface coverage. Their model however, did not predict the experimentally observed maximum in the critical shear rate.

In the present article, we develop our tube model further to account for the effects of higher grafting density of end-tethered chains. The motivation for this work is threefold. First, we wish to investigate the case of high surface coverage at which different tethered chains might start to become entangled with each other since this has not been done before to the best of our knowledge. Second, we wish to attempt to make quantitative comparisons between the predictions of the tube model and microscopic as well as macroscopic experimental data on slip. Third, the high surface coverage regimes deserve investigation because they represent more closely the situation in a real extrusion scenario. This article is structured as follows. In Sec. II we will discuss the various surface coverage regimes and we will derive the tube model for the interfacial region that is coupled with the bulk. In Sec. III we will discuss the general predictions of the model, the various scaling laws for slip parameters under the different surface coverage regimes and provide a quantitative comparison between predictions and experimental data. Section IV summarizes the conclusions of the work.

II. THEORY

A. Regimes of surface coverage

We consider the case of monodisperse molecules of N' monomers (N segments) per molecule, which are end tethered to a solid wall and are entangled with monodisperse bulk chains of P' monomers (P segments) per molecule such that $P' > N'$. Let N_e be the number of monomers between consecutive entanglements such that $N = N'/N_e$ and $P = P'/N_e$. Further, we suppose that there are $\Sigma = \sigma/a'^2$ molecules per unit area tethered to the wall, where a' is the monomeric length scale and σ is the dimensionless surface coverage. The layer of tethered chains at the wall is called the interfacial region and is denoted by subscript *I*. Similarly, the *P* chains away from the wall constitute the bulk, which is denoted by subscript *B*. The interfacial region has a thickness h which

depends on the surface coverage; for $P' > N'$ the thickness of the interfacial region remains unchanged at $h = a'\sqrt{N'}$ for all regimes until the system enters the dry brush regime [Leger *et al.* (1999)].

At very low values of surface coverage, i.e., in the so-called mushroom regime, different tethered chains do not become entangled with each other and all of their entanglements form with the bulk chains. Since each tethered chain has N'/N_e entanglements, the number of bulk chains per unit area trapped by the tethered chains is given by

$$\Sigma_P = \frac{N'}{N_e}\Sigma. \tag{1}$$

The volume fraction of the tethered chains (ϕ_T) in the interfacial region of thickness h is given by

$$\phi_T = \frac{a'^3 N'\Sigma}{h} = \frac{a'N'\sigma}{h}. \tag{2}$$

In the absence of any tethered chains the number density of bulk chains in a skin of thickness $R_p = a'\sqrt{P'}$ near the wall would be given by

$$\Sigma_p = R_p/a'^3 P' = 1/(a'^2\sqrt{P'}). \tag{3}$$

When the wall has Σ tethered chains per unit area the number of bulk chains near the wall would be given by

$$\Sigma_P = (R_P - \phi_T h)/a'^3 P', \tag{4}$$

or from Eq. (2),

$$\sigma_P = a'^2\Sigma_p = (\sqrt{P'} - N'\sigma)/P'.$$

When all of these chains are entangled with the tethered chains such that each bulk chain makes on average only one entanglement with a tethered chain, then Eqs. (1) and (4) can be equated to give the maximum surface coverage σ_c to which the mushroom regime extends. Thus,

$$\sigma_c = \frac{N_e\sqrt{P'}}{N'(P' + N_e)}. \tag{5}$$

Note that at $\sigma = \sigma_c$, $\phi_T = 1/\sqrt{PN} \ll 1$ [from Eq. (2)]. Thus even after the mushroom regime the interfacial region is occupied by mostly bulk chains. Equation (5) gives a slightly different value for the critical surface coverage σ_c than that estimated by Brochard-Wyart *et al.* (1996), who ignored the presence of tethered chains in calculating the number of bulk chains near the wall.

For $\sigma > \sigma_c$, each bulk chain starts making on average more than one entanglement with the tethered chains. Let χ be the average number of entanglements that one bulk chain makes with the tethered chains so that $\chi\Sigma_P$ are the total number of entanglements made by bulk chains with tethered chains per unit area. Since the total number of entanglements made by the tethered chains per unit area is $(N'/N_e)\Sigma$, the fraction of the number of entanglements that the tethered chains make with the bulk chains, ϕ, is given by

$$\phi = \frac{\chi\Sigma_P}{(N'/N_e)\Sigma} = \frac{\chi\sigma_P}{(N'/N_e)\sigma}. \tag{6}$$

It can easily be shown from Eq. (4) that, in the mushroom regime ($\sigma \leqslant \sigma_c$), since $\sigma \ll \sigma_P$, every entanglement of the tethered chains is made with a separate bulk chain. For surface coverage above the mushroom regime, the tethered chains continue to become entangled only with bulk chains, i.e., $\phi = 1$, however, the average number of entanglements χ that one bulk chain makes with the tethered chains increases with the surface coverage until surface coverage σ_o is reached at which $\chi = N'/N_e$. These are the maximum number of entanglements possible between the bulk and a tethered chain; any further increase in Σ will result in entanglements between tethered chains. The value of σ_o can be obtained simply by putting $\phi = 1$ and $\chi = N'/N_e$ in Eq. (6). Thus,

$$\sigma_o = \frac{\sqrt{P'}}{N' + P'}. \tag{7}$$

Above σ_o, ϕ is given by

$$\phi = \frac{\sigma_P}{\sigma} = \frac{\Sigma_P}{\Sigma} = \frac{\sqrt{P'} - N'\sigma}{P'\sigma}, \tag{8}$$

which shows that the fraction of entanglements between tethered chains and bulk chains decrease with a further increase in surface coverage. In fact, as $\sigma \to N'^{-0.5}$ the volume fraction of tethered chains in the interfacial region tends toward unity $\phi_T \to 1$. Thus, the bulk chains are driven out of the interfacial region and this is called the dry brush regime [Leger *et al.* (1999)].

In summary, there are four regimes of surface coverage and they are defined below.

(1) Regime I ($\sigma \leqslant \sigma_c$): The *mushroom* regime in which tethered chains are independent of each other and each bulk chain makes on average only one entanglement with a tethered chain. σ_c is given by Eq. (5).
(2) Regime II ($\sigma_c < \sigma \leqslant \sigma_o$): A *cooperative* regime in which tethered chains do not become entangled with each other and each bulk chain makes on average $1 < \chi < N$ entanglements with the tethered chains. σ_o is defined by Eq. (7).
(3) Regime III ($\sigma_o < \sigma < N'^{-0.5}$): An overlap regime in which tethered chains start to become entangled with each other.
(4) Regime IV ($\sigma > N'^{-0.5}$): The *dry brush* regime.

Figure 1 shows the various regimes of surface coverage for the case of polydimethylsiloxane (PDMS, $N_e = 183$) and for $P > N$ ($P = 72, N = 7$). The case of $P \leqslant N$ is discussed elsewhere [Leger *et al.* (1999)] and is beyond the scope of the present discussion.

B. Interfacial plateau modulus

In the mushroom regime the high frequency modulus of the interfacial region ($G^o_{N,I}$) is given by [Joshi *et al.* (2001)]

$$G^o_{N,I} = \frac{\Sigma}{a} kT, \tag{9}$$

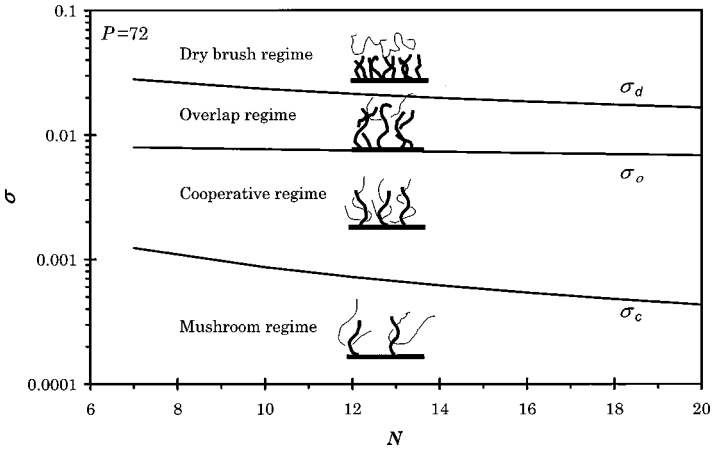

FIG. 1. Regimes of surface coverage for polydimethylsiloxane: (a) at constant bulk molecular weight and varying chain lengths of tethered chains; (b) at constant molecular weight of the tethered chain and varying chain lengths of bulk chains.

where a is the segment length or tube diameter ($= a'\sqrt{N_e}$), k is the Boltzmann constant and T is the absolute temperature. The subscript I stands for the interfacial region. Equation (9) is also valid for regime II.

For higher surface coverage in regime III only that fraction of the total entanglements in the interfacial region which the tethered chains make with the bulk chains is active in transferring stress between the interfacial region and the bulk. Hence, the interfacial modulus can be written as

$$G^o_{N,I} = \phi \frac{\Sigma}{a} kT, \tag{10}$$

where $\phi = 1$ for $\sigma \leqslant \sigma_o$ and ϕ is given by Eq. (8) for $\sigma > \sigma_o$. Accordingly, Eq. (10) can be written as

$$\begin{aligned} G^o_{N,I} &= \frac{\sigma}{a'^3\sqrt{N_e}} kT, \quad \sigma < \sigma_o, \\ G^o_{N,I} &= \frac{\sqrt{P'} - N'\sigma}{a'^3 P' \sqrt{N_e}} kT, \quad \sigma > \sigma_o. \end{aligned} \tag{11}$$

The interfacial plateau modulus increases with σ in regimes I and II. Above σ_o, it starts decreasing as the bulk chains are progressively expelled from the interfacial region. For $\sigma > N'^{-0.5}$, the bulk chains are almost completely expelled from the interfacial region.

C. Dynamics in the mushroom regime

We now consider the case where the bulk chains have a nonzero velocity V_s at the wall. The tethered chains, which are entangled with the bulk chains, resist the flow of the bulk molecules. A tube model describing the dynamics of tethered chains in the mushroom regime has been discussed by Joshi *et al.* (2001). In that model the tethered chains are assumed to experience an apparent shear rate $\kappa_{12,I} \sim \tilde{V}_s/h$. At low shear rates, the

tethered chains experience constraint release relaxation caused by reptation of the bulk chains. In this linear regime the interfacial stress increases with the interfacial shear rate until

$$\kappa_{12,I}^{*} = \frac{V_s^{*}}{a\sqrt{N}} \sim \frac{1}{\tau_{\mathrm{CR},I}}. \tag{12}$$

The constraint release (CR) time scale is given by $\tau_{\mathrm{CR},I} \approx N^2 \tau_d(P)$, where $\tau_d(P)$ is the reptation time of the bulk chain. The diffusion coefficient for the tethered chains due to the CR process is given by [Watanabe (1999)]

$$D_{\mathrm{CR}} = 2L_I^2/(\pi^2 \tau_{\mathrm{CR},I}), \tag{13}$$

where L_I is the contour length of the tethered chain.

The relaxation due to CR occurs simultaneously with arm retraction (AR), which becomes particularly significant for short tethered chains ($N < 10$). In the arm retraction process, the tethered chain retracts its tail (free end) into its own tube and then restores its configuration by moving outward again in a new tube. Relaxation of the segments nearer to the tethered end occurs more slowly than that for the segments at the free end. For a tail of K segments, the relaxation time due to AR is given by [Ajdari *et al.* (1994)]

$$\tau_{\mathrm{AR},I}(K,N) \approx N^{-1} \tau_d(N) \exp(\mu K^2/N), \tag{14}$$

where $\mu = 15/8$ and the corresponding diffusion coefficient is given by

$$D_{\mathrm{AR}}(K) = \frac{a^2}{\pi^2 \tau_{\mathrm{AR},I}}. \tag{15}$$

Since the CR and AR processes occur in parallel, the diffusion coefficient is given by

$$D_I = D_{\mathrm{CR}} + D_{\mathrm{AR}}. \tag{16}$$

It should be noted that the approach developed in this article differs from earlier theory [Joshi *et al.* (2001)], in which we had considered that either AR or CR acts independently depending on the molecular weight of the tethered chain.

Above the critical shear rate or the critical slip velocity given by Eq. (12) the tethered chains are easily oriented by the flowing bulk chains. This is because the tethered chains experience highly suppressed convective constraint release (CCR) relaxation, which is unable to randomize their orientation caused by the flowing bulk chains. The rate at which constraints on the tethered chains are released by the convection of bulk chains is proportional to $\kappa_{12,B}$, whereas the rate at which the tethered chains deform is proportional to $\kappa_{12,I}$. For large values of slip velocity, since $\kappa_{12,I} > \kappa_{12,B}$, the tethered chains can easily be oriented. Contrary to this the molecules in the bulk are less susceptible to orientation because of the more effective CCR process.

At high shear rates corresponding to approximately $\kappa_{12,I} > 1/\tau_{R,I}(N)$, where $\tau_{R,I}(N)$ is the longest Rouse relaxation time, the tethered chains undergo stretching and simultaneously try to relax their stress by partial retraction. The overall flow curve near the wall shows significant nonmonotonic behavior, which implies interfacial instability.

D. Dynamics at higher grafting densities

At grafting densities in regimes II and III the dynamics of individual tethered chains are coupled with those of the neighboring tethered chains. In regime II as the number of tethered chains increases, a bulk chain is forced to form more than one entanglement with

a tethered chain as shown in Fig. 1. Consequently, reptation of a bulk chain simultaneously releases several constraints on a tethered chain. This scenario is similar to the case of a star polymer (of N segments per arm) entangled with linear chains of P segments per chain, for which Brochard-Wyart *et al.* (1994) proposed the terminal time for constraint release of the star arm to be $\tau_{\mathrm{CR}} \approx N^2 \tau_d(P)/f$, where f is the number of entanglements along the arm of the star released by a single neighboring bulk chain reptating along its length. Different expressions for estimating factor f were proposed by Brochard-Wyart *et al.* (1994) depending on whether the star-linear blend mixture belongs to the Stokes regime or to the Rouse regime and this led to different scaling relations for τ_{CR}, which agreed better with experimental data.

By analogy with the above case, the reptation of a single bulk chain in regime II releases χ number of constraints on a tethered chain. Hence, the CR time scale for a tethered chain in the interfacial region $\tau_{\mathrm{CR},I}$ is given by

$$\tau_{\mathrm{CR},I}(N) \approx N^2 \tau_d(P)/\chi. \tag{17}$$

The determination of $\tau_{\mathrm{CR},I}$ differs slightly from that in the Brochard-Wyart *et al.* (1994) analysis since the value of χ can be estimated in the present case from knowledge of the surface coverage. As discussed earlier, the value of χ is unity until a critical surface coverage (σ_c) is reached. Above σ_c, χ starts increasing until an overlap surface coverage (σ_o) is reached, and above which it remains locked at N'/N_e. From Eqs. (4) and (6) χ can be written as

$$\chi = 1, \quad \sigma < \sigma_c,$$

$$\chi = \frac{\sigma N' P'}{N_e(\sqrt{P'} - N'\sigma)}, \quad \sigma_c < \sigma < \sigma_o, \tag{18}$$

$$\chi = N'/N_e, \quad \sigma > \sigma_o.$$

Thus, the time scale for CR is constant until a critical surface coverage (σ_c) is reached. Above σ_c in regime II, τ_{CR} decreases with an increase in surface coverage. This implies that the tethered chains cooperatively relax faster without becoming entangled with each other. Above σ_o in regime III the CR time is equal to $\tau_{\mathrm{CR},I}(N) \approx N\tau_d(P)$ and is independent of the surface coverage. The expression for the CR time scale is given by

$$\tau_{\mathrm{CR},I}(N) = N^2 \tau_d(P), \quad \sigma < \sigma_c,$$

$$\tau_{\mathrm{CR},I}(N) = \frac{N(\sqrt{P/N_e} - N\sigma)}{P\sigma}\tau_d(P), \quad \sigma_c < \sigma < \sigma_o, \tag{19}$$

$$\tau_{\mathrm{CR},I}(N) = N\tau_d(P), \quad \sigma > \sigma_o.$$

Finally, it can be argued that the convection of bulk chains at higher shear rates will also release χ constraints on a tethered chain so that the times scale for CCR relaxation will also be affected in regime II in a manner similar to that in the CR time scale.

E. Constitutive equation

Details of the constitutive equation for tethered chains in the mushroom regime were presented earlier [Joshi *et al.* (2001)]. In the following we will first summarize the essential aspects of the previous model and then extend it to the case of higher grafting densities in regimes II and III. In an isothermal steady extrusion experiment the control

variable is either the apparent wall shear rate or the wall shear stress, while the slip velocity is measured or inferred from the data. Correspondingly, the objective of our model is to predict the slip velocity for an imposed bulk shear rate near the wall or for an imposed wall shear stress. The other associated slip parameters such as the slip length, the critical wall shear stress and the critical bulk shear rate follow directly from the predicted/measured slip velocity. It is important to recognize that the dynamics of the tethered chains are inherently coupled with the dynamics of the bulk chains through the continuity of shear stress. Hence, the shear stress predicted from a constitutive equation for bulk molecules experiencing a bulk shear rate $\kappa_{12,B}$ near the wall should be equal to the shear stress predicted from a constitutive equation for tethered chains experiencing an interfacial slip velocity V_s.

We have used the constitutive equation of the contour variable model [Mead *et al.* (1998)] for the bulk molecules. For a detailed description of the equations, the reader is referred to the original CV model. At steady state, the constitutive equation for shear stress σ_{12} consists of a set of coupled integrodifferential equations given by

$$\sigma_{12,B} = \frac{15}{4} G^0_{N,B} \frac{1}{L_{0,B}} \int_{-L_{0,B}/2}^{L_{0,B}/2} q_B^2 S_{12,B}(s_0) ds_0, \tag{20}$$

$$\frac{\partial q_B(s_0)}{\partial s_0} = \frac{1}{6PD_{\text{rep},P}} \left(2 \frac{\langle v_B \rangle|_{s_0 = L_B/2}}{L_B} \right) (s - s_0) - \frac{\langle v_B(s) \rangle}{3PD_{\text{rep},P}}, \tag{21}$$

$$S_{12,B}(s) = \int_0^\infty \frac{\partial G_B(s,\theta)}{\partial \theta} Q_{12,B}[E_{\mathbf{B}}(\theta)] d\theta, \tag{22}$$

$$\frac{\partial G_B(s,\theta)}{\partial \theta} = D_{\text{rep},P} \frac{\partial^2 G_B(s,\theta)}{\partial s^2} - \langle v_B(s) \rangle \frac{\partial G_B(s,\theta)}{\partial s} - f(q_B) \left(2 \frac{\langle v_B \rangle|_{s_0 = L_B/2}}{L_B} \right) G_B(s,\theta) - \frac{G_B(s,\theta)}{\tau_{\xi,B}(s)}. \tag{23}$$

In the above equations, $D_{\text{rep},P} = L_B^2/[\pi^2 \tau_d(P)]$ is the longitudinal diffusivity of the bulk chain. L_B is the contour length of the bulk chain at any given deformation rate. $G_B(s,\theta)$ is the segment renewal probability for the bulk chain at time θ and at position s. $G^o_{N,B}$ is the high frequency plateau modulus of the bulk chains. $L_{0,B} = aP$ is the equilibrium contour length of a bulk chain, a being the tube diameter or the length of a segment. $S_{12,B}$ is the shear component of the orientational order parameter tensor $S_{\mathbf{B}}$. s_0 is the undeformed reference coordinate of the contour length ($s_0 = \pm L_{0,B}/2$ at the chain ends and $s_0 = 0$ at the center), while s is the reference coordinate of the deformed contour length. q_B is the segmental stretch ratio defined as $q_B = \partial s/\partial s_0$. $\langle v_B(s) \rangle$ is the continuous retraction velocity of a bulk chain along its contour directed towards its center given by

$$\langle v_B(s) \rangle = \kappa_{\mathbf{B}} : \int_0^s S_{\mathbf{B}}(s') ds' = \kappa_{12,B} \int_0^s S_{12,B}(s') ds'. \tag{24}$$

$E_{\mathbf{B}}(\theta)$ is the deformation tensor for bulk chains and $Q_{\mathbf{B}}$ is the geometric universal tensor defined as

$$Q_{\mathbf{B}} = \langle (E_{\mathbf{B}} \cdot \mathbf{u})(E_{\mathbf{B}} \cdot \mathbf{u})/|E_{\mathbf{B}} \cdot \mathbf{u}| \rangle / |E_{\mathbf{B}} \cdot \mathbf{u}| \rangle - \mathbf{I}/3,$$

where $\langle\ \rangle$ denotes the average over the isotropic distribution of unit vectors **u** and **I** is the unit tensor. Finally, $\tau_{\xi,B}$ is the fluctuation time scale of the bulk chains and is given by

$$\tau_{\xi,B}(s) = (\tau_R(P)/4)\exp(0.5\vartheta P\xi_B^2), \tag{25}$$

where $\xi_B = 1-2|s|/L_B$, $\vartheta = 1.5$ and $\tau_R(P)$ is the longest Rouse time of the bulk chain.

The initial and boundary conditions for Eqs. (21) and (23) are

$$G_B(s_0) = 1, \quad \text{at } \theta = 0 \text{ (initial condition)},$$

$$G_B(\theta) = 0, \quad \text{at } s_0 = \pm L_{0,B}/2 \text{ (due to fluctuations at the chain end)},$$

$$\frac{dG_B(\theta)}{ds_0} = 0, \quad \text{at } s_0 = 0 \text{ (symmetry at the center of the chain)},$$

$$q_B = 1, \quad \text{at } s_0 = \pm L_{0,B}/2 \text{ (the chain ends are always random)}.$$

The procedure for solving this set of equations is summarized in the Appendix.

The constitutive equation for tethered chains can be developed from the CV model by incorporating the discussions of Secs. II C and II D. The set of integrodifferential equations for the tethered chains can be given by

$$\sigma_{12,I} = \frac{15}{4}G_{N,I}^0\frac{1}{L_{0,I}}\int_0^{L_{0,I}} q_I^2 S_{12,I}(s_0)ds_0, \tag{26}$$

$$\frac{\partial q_I(s_0)}{\partial s_0} = \frac{1}{6ND_{\text{rep},N}}\left(2\frac{\langle v_2\rangle}{L_B}\right)(s-s_0) - \frac{\langle v_1(s_0)\rangle}{3ND_{\text{rep},N}}, \tag{27}$$

$$S_{\mathbf{I}}(s_0) = \int_0^{\infty}\frac{\partial G_I(s_0,\theta)}{\partial\theta}Q_{\mathbf{I}}(E_{\mathbf{I}}(\theta))d\theta, \tag{28}$$

$$\frac{\partial G_I(s,\theta)}{\partial\theta} = D_{\text{eff}}\frac{\partial^2 G_I(s,\theta)}{\partial s^2} - \langle v_1(s)\rangle\frac{\partial G_I(s,\theta)}{\partial s} - f(q_I)\left(2\frac{\chi\langle v_2\rangle\phi}{L_B}\right)G_I(s,\theta) - \frac{G_I(s,\theta)}{\tau_{\xi,I}(s)}. \tag{29}$$

In Eq. (26) the value of the interfacial plateau modulus depends on the regime of surface coverage as given by Eq. (11). The segment renewal probability for the tethered chains, G_I, is governed by the different relaxation mechanisms discussed earlier, namely, CR and AR at low shear rates, CCR in the intermediate shear rate regime and contour length fluctuations at high shear rates. We consider a general case of dimensionless surface coverage σ, for which a fraction ϕ of the total entanglements in the interfacial region is formed between tethered chains and bulk chains and the remaining $1-\phi$ is formed between neighboring tethered chains. Since a tethered chain cannot reptate, only a fraction ϕ of its tube can relax by the CR process at low shear rates. The AR process also occurs in parallel to the CR relaxation for this fraction of the tube. The remaining $1-\phi$ of the tube can relax only by the AR process. The first term on the right in Eq. (29) is the contribution from the parallel CR and AR processes. The effective diffusivity of the tethered chains can then be given by

$$D_{\text{eff}} = \phi D_I + (1-\phi)D_{\text{AR}} = \phi D_{\text{CR}} + D_{\text{AR}}, \tag{30}$$

where D_{CR} and D_{AR} are given by Eqs. (13) and (15). The arm retraction and constraint release time constants are given in Eqs. (14), (17), and (18).

The second term in Eq. (29) arises from continuous retraction of the chain within its tube at an average relative velocity given by

$$\langle v_1(s_o)\rangle = \phi V_s + \kappa_{12,I}\int_0^s S_{12,I}(s')ds'. \tag{31}$$

We have assumed here that the relative velocity V_s applies only to the fraction ϕ of the tube since the tethered chains experience no relative slip velocity with respect to each other. The relationship between slip velocity and the interfacial shear rate is given by

$$V_s = h\kappa_{12,I}. \tag{32}$$

The third term in Eq. (29) gives the contribution of the convective constraint release process. The time scale for the CCR process is given approximately by $L_B/(\chi\langle v_2\rangle)$, where the factor χ accounts for the number of constraints on a tethered chain released by convection of a single bulk chain end. The factor ϕ in the CCR term accounts for that fraction of the tube released by convection of bulk chains. The velocity of convection of the bulk chain is given by

$$\langle v_2\rangle = \kappa_{12,B}\int_0^{L_B/2} S_{12,B}(s')ds'. \tag{33}$$

Note that the constitutive equation for the tethered chains is coupled with the constitutive equation for the bulk through the CCR terms in Eqs. (33) and (29) besides the stress continuity condition.

The last term in Eq. (29) represents the contribution from contour length fluctuations. $\tau_{\xi,I}(s)$ is the time scale for fluctuations given by

$$\tau_{\xi,I}(s) = [\tau_R(N)]\exp(\vartheta N\xi_I^2), \tag{34}$$

where $\xi_I = 1-2|s|/L_I$, $\vartheta = 1.5$ and $\tau_R(N)$ is the longest Rouse time of the tethered chain. Note that the fluctuation time for a tethered chain is four times slower than that for a free chain of the same molecular weight [Joshi *et al.* (2001)].

The initial and boundary conditions for Eqs. (27) and (29) are

$$G_I(s_0) = 1, \quad \text{at } \theta = 0 \text{ (initial condition)},$$

$$G_I(\theta) = 0, \quad \text{at } s_0 = L_{0,I} \text{ (due to fluctuations at the chain end)},$$

$$\frac{dG_I(\theta)}{ds_0} = 0, \quad \text{at } s_0 = 0 \text{ [for discussion, see Joshi } et\ al. \text{ (2001)]},$$

$$q_I = 1, \quad \text{at } s_0 = L_{0,I} \text{ (the chain ends are always random)}.$$

Other terms in the constitutive equation for tethered chains such as the geometrical universal tensor $Q_{\mathbf{I}}$, the deformation tensor $E_{\mathbf{I}}(\theta)$ and the reptation diffusion coefficient $D_{\text{rep},N}$ are defined in a similar manner to those for bulk chains.

Finally, the constitutive equations for the bulk and the interfacial region are coupled through the continuity of stress boundary condition, namely,

$$\sigma_{12,I} = \sigma_{12,B}. \tag{35}$$

The procedure for solving this large set of simultaneously coupled integrodifferential equations is outlined in the Appendix. It essentially allows the calculation of the interfa-

cial slip velocity V_s at a specified bulk shear rate near the wall or of a specified wall shear stress. Other slip parameters can then be calculated in a straightforward manner. The model parameters are the number of entanglements per chain for the bulk molecules (P), the number of entanglements per chain for the tethered molecules (N), the reptation time (τ_d) of the bulk chain, the plateau modulus of the bulk $G^0_{N,B}$ and the surface coverage (Σ). The plateau modulus can be determined from independent rheological experiments and has been documented for several polymers [Fetters *et al.* (1994)]. The reptation time for the bulk chains can be estimated from $\tau_d(P) = (12/\pi^2)\,\eta_{0,B}/G^0_{N,B}$. $\eta_{0,B}$ is the zero shear viscosity of the bulk, which can be measured by low strain rate experiments. The wall shear stress in all of the calculations presented below has been nondimensionalized using the bulk plateau modulus. Similarly, the slip velocity has been nondimensionalized using the reptation time of the bulk chain and the equilibrium contour length of the bulk chain unless stated otherwise.

III. PREDICTIONS

A. Scaling relationships

The tube model presented in Sec. II predicts simple scaling relationships between the critical slip parameters and the experimental control parameters for the different surface coverage regimes. The slip velocity at the onset of strong slip can be defined as

$$V_s^* \sim h/\tau, \tag{36}$$

where τ is an appropriate relaxation time that governs the onset of strong slip. Further, from Eq. (26) the critical shear stress can be given by

$$\sigma^*_{12,I} = G^0_{N,I} \max\left(\frac{1}{L_{0,I}}\int_0^{L_{0,I}} q_I^2 S_{12,I} ds\right) \sim G^0_{N,I}. \tag{37}$$

The critical slip length at the onset of strong slip can be defined as

$$b_0 = \frac{\eta_{0,B}}{k'} = \frac{\eta_{0,B}}{\sigma^*_{12,I}/V_s^*} \sim \frac{\eta_{0,B}}{G^0_{N,I}/(h/\tau)} \sim \frac{G^0_{N,B}\tau_d(P)h}{G^0_{N,I}\tau} \sim a\sqrt{N}\frac{G^0_{N,B}}{G^0_{N,I}}\frac{\tau_d(P)}{\tau}, \tag{38}$$

where k' is a friction coefficient at the wall.

The critical shear rate is given by

$$\kappa^*_{12,B} = \frac{V_s^*}{b^*} \sim \frac{G^0_{N,I}}{G^0_{N,B}\tau_d(P)}. \tag{39}$$

The bulk modulus can be estimated from [Graessley (1974)]

$$G^0_{N,B} = \frac{\sqrt{N_e}kT}{a^3}. \tag{40}$$

Consequently, the ratio of the interfacial modulus to the bulk modulus can be obtained from Eqs. (11) and (40) as

$$\frac{G^0_{N,I}}{G^0_{N,B}} = \sigma\sqrt{N_e}, \quad \sigma < \sigma_o,$$
$$\frac{G^0_{N,I}}{G^0_{N,B}} = \frac{\sqrt{P'} - N'\sigma}{P'}\sqrt{N_e}, \quad \sigma > \sigma_o. \tag{41}$$

For $N > 10$ the onset of strong slip is dictated by the CR time scale, which is given by Eq. (19). From the above discussion the following scaling relationships can be derived for the three regimes of surface coverage.

1. Mushroom regime ($\sigma < \sigma_c$)

$$V_s^* \sim \frac{h}{\tau_{\mathrm{CR},I}(N)} \sim N^{-1.5}P^{-3.4}. \tag{42}$$

For shorter tethered chains of $N < 10$, $V_s^* \sim [h/\tau_{\mathrm{AR},I}(N)] \sim N^{-1.5}\exp(-2N)$,

$$\sigma^*_{12,I} \sim G^0_{N,I} \sim \sigma T, \tag{43}$$

$$b_0 \sim a\sqrt{N}\frac{G^0_{N,B}}{G^0_{N,I}}\frac{\tau_d(P)}{\tau_{\mathrm{CR},I}(N)} \sim N^{-1.5}\sigma^{-1}. \tag{44}$$

For shorter tethered chains of $N < 10$, $b_0 \sim N^{-1.5}\exp(-2N)P^{3.4}\sigma^{-1}$,

$$\kappa^*_{12,B} \sim \frac{G^0_{N,I}}{G^0_{N,B}\tau_d(P)} \sim \sigma P^{-3.4}. \tag{45}$$

2. Cooperative regime ($\sigma_c < \sigma < \sigma_o$)

$$V_s^* \sim \frac{h}{\tau_{\mathrm{CR},I}(N)} \sim \chi N^{-1.5}P^{-3.4}, \tag{46}$$

where $1 < \chi < N$ as per Eq. (18).
For $P' \gg N' > N_e$ the above relationship simplifies to $V_s \sim \sigma N^{-0.5}P^{-2.9}$. Note that this relationship is identical to the one derived by Brochard-Wyart *et al.* (1996).

For shorter chains of $N < 10$, $V_s^* \sim h/\tau_{\mathrm{AR},I}(N) \sim N^{-1.5}\exp(-2N)$,

$$\sigma^*_{12,I} \sim G^0_{N,I} \sim \sigma T, \tag{47}$$

$$b_0 \sim \chi N^{-1.5}\sigma^{-1}. \tag{48}$$

For shorter tethered chains of $N < 10$, $b_0 \sim N^{-1.5}\exp(-2N)P^{3.4}\sigma^{-1}$.

Again for $P' \gg N' > N_e$ the scaling simplifies to $b_c \sim P^{0.5}$,

$$\kappa^*_{12,B} \sim \sigma P^{-3.4}. \tag{49}$$

3. Overlap regime ($\sigma > \sigma_o$)

$$V_s^* \sim \frac{h}{\tau_{\mathrm{CR},I}(N)} \sim N^{-0.5}P^{-3.4}. \tag{50}$$

For shorter tethered chains of $N < 10$, $V_s^* \sim [h/\tau_{\mathrm{AR},I}(N)] \sim N^{-1.5}\exp(-2N)$,

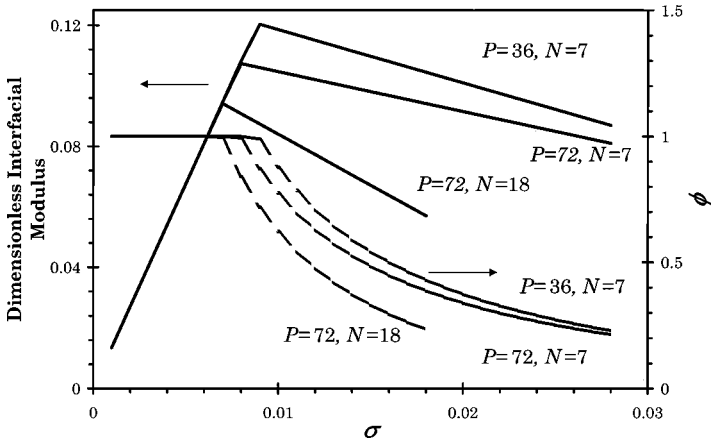

FIG. 2. Interfacial modulus and fraction of the total entanglements in the interfacial region that are formed between tethered chains and bulk chains for increasing values of the surface coverage.

$$\sigma^*_{12,I} \sim G^0_{N,I} \sim \frac{\sqrt{P}-N\sigma\sqrt{N_e}}{P}T \sim P^{-0.5}T, \quad \text{for } P' \gg N' > N_e, \tag{51}$$

$$b_0 \sim \frac{P}{\sqrt{PN}-N^{1.5}\sigma\sqrt{N_e}} \sim P^{0.5}N^{-0.5}. \tag{52}$$

For shorter tethered chains of $N < 10$, $b_0 \sim N^{-1.5}\exp(-2N)P^{3.9}$,

$$\kappa^*_{12,B} \sim (\sqrt{P}-N\sigma\sqrt{N_e})P^{-4.4} \sim P^{-3.9}. \tag{53}$$

In Secs. III B–III D we present the results obtained by solving the full set of constitutive equation developed in Sec. II. The calculations were performed for a PDMS melt with $N_e = 183$.

B. Interfacial high frequency modulus

Figure 2 shows a plot of the dimensionless interfacial plateau modulus and ϕ versus the dimensionless surface coverage for the case of $P = 72$ and $N = 7$ and 18. Note from Fig. 1(a) that $\sigma_o = 0.008$ for $N = 7$ and $\sigma_o = 0.007$ for $N = 18$. The interfacial plateau modulus is nondimensionalized using bulk plateau modulus $G^0_{N,B}$ ($= \sqrt{N_e}k_BT/a^3$). Of the total entanglements in the interfacial regime, the fraction ϕ that is formed between the bulk and tethered chains is equal to unity at low surface coverage (regimes I and II) and decreases after the surface coverage increases beyond $\sigma = \sigma_o$ (regime III). Correspondingly, the interfacial plateau modulus increases with the surface coverage until $\sigma = \sigma_o$, after which it decreases since only a fraction ϕ of the total entanglements is responsible for sharing the stress between the bulk and tethered chains.

C. Flow curves

In Figs. 3(a)–3(c), the dimensionless wall shear stress experienced by tethered chains is plotted versus the dimensionless slip velocity for various values of N keeping $P = 72$ and the surface coverage constant. It is equally possible to plot the dimensionless interfacial wall shear rate on the X axis since V_s and κ_I are related by Eq. (32). Figure

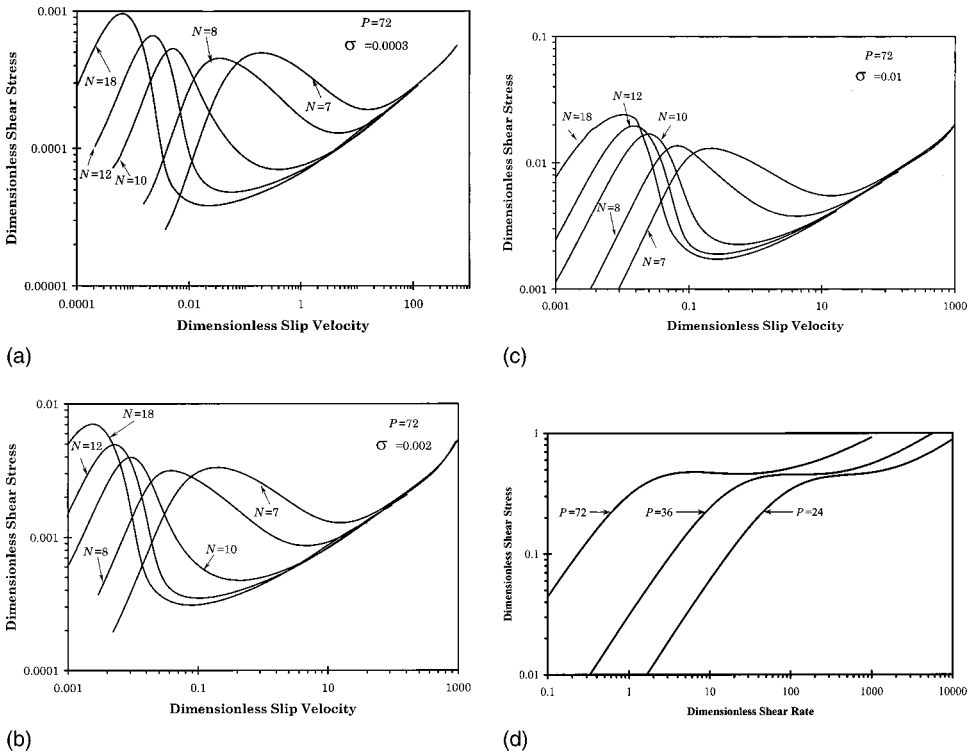

FIG. 3. Flow curves for tethered chains of varying molecular weights entangled with bulk chains of length $P = 72$: (a) mushroom regime, (b) cooperative regime and (c) overlap regime. The slip velocity was nondimensionalized by the reptation time and the equilibrium contour length of the free chain with 72 segments. (d) Flow curves of bulk chains of three different molecular weights for comparison with the flow curves of tethered chains. The shear rate is nondimensionalized using the reptation time of the chain with 72 segments.

3(a) corresponds to the mushroom regime ($\sigma = 0.0003$), Fig. 3(b) corresponds to the cooperative regime ($\sigma = 0.002$) and Fig. 3(c) corresponds to the overlap regime ($\sigma = 0.01$). Figure 3(d) shows the flow curves for bulk chains (prediction of the counter-variable model with fluctuations) of three different molecular weights. It is clearly seen that, while the bulk flow curves are monotonic in nature, those for the tethered chains are strongly nonmonotonic. This is due to the fact that the CCR mechanism facilitates rapid relaxation of the bulk chains and prevents them from fully orienting in the flow direction even at high shear rates, whereas the tethered chains experience only restricted CCR relaxation near the wall that is ineffective in randomizing their orientation at high shear rates. The role of CCR was explained in detail by Joshi *et al.* (2001). The nonmonotonic nature of the flow curve for the tethered chains implies interfacial flow instability, which can give rise to flow and pressure oscillations in a controlled rate extrusion and a discontinuous jump in flow rate for controlled stress extrusion. The discontinuous jump in flow rate is associated with a ''coil-to-stretch'' transition of the tethered chains [Joshi *et al.* (2001)].

Figures 3(a)–3(c) show that the critical slip velocity, which corresponds to the velocity at the stress maximum, decreases with an increase in N, the decrease being more rapid in the mushroom regime than in the cooperative and overlap regimes. The critical shear stress is seen to increase slightly with N, although the scaling relationships [Eqs. (43) and (47)] do not indicate such a trend. The increase in critical stress with N can be expected

since longer molecules relax more slowly and thereby retain relatively larger portions of their original tubes; hence they have a greater magnitude of orientation order tensor $S_{12,I}$. Thus the value of the integral in Eq. (37) is higher for longer chains, which results in an increase in critical stress with N. It may also be noted from Figs. 3(a)–3(c) that for a given value of N the critical stress increases with the surface coverage. This is expected since the interfacial modulus increases with σ. However, above the overlap coverage the critical stress decreases again as will be seen later. Finally, the nonmonotonicity of the flow curve decreases with a decrease in N. This happens due to easier randomization of low molecular weight tethered chains. This implies that the magnitude of the stick–slip transition decreases if the surface happens to have preferentially low molecular species adsorbed on it. The flow curves for various P keeping $N = 18$ and $\sigma = 0.0003$, 0.002, and 0.01 constant have similar features and are shown in Figs. 4(a)–4(c). In Fig. 4 the critical slip velocity has been nondimensionalized with the reptation time and contour length of the tethered chain. The critical slip velocity is found to decrease with an increase in P and the nonmonotonic nature of the flow curve increases with P. The critical stress is weakly dependent on P in regimes I and II and shows a stronger dependence on P in regime III.

Figures 5(a)–5(c) show the scaling relationships extracted from the flow curves of Figs. 3 and 4 for the three values of surface coverage that correspond to the three regimes. Several features in this plot are worth discussing. The critical slip velocity decreases almost exponentially with an increase in N for $N < 10$ and then follows a slower power law decrease for higher N. The rapid exponential decrease arises from the arm retraction process for short chains and the power law relationships originate from the constraint release process. Both trends are in agreement with the scaling laws derived earlier. Note also that for a given $N(N > 10)$ the critical slip velocity increases with an increase in surface coverage. This is evidently due to the fact that it becomes increasingly more difficult for the bulk chains to orient the tethered chains because of the cooperatively faster constraint release relaxation in regimes II and III. For $N < 10$ this effect is not observed since the arm retraction process is not cooperative and hence does not depend on the surface coverage. Note also that there is a smooth transition of the critical slip velocity between short and long tethered chains, indicating that both arm retraction and constraint release processes are active for the intermediate chain lengths. The critical slip velocity decreases as P^{-3} in regimes I and II and as $P^{-3.9}$ in regime III, which is in agreement with the scaling laws presented earlier. The critical stress increases slightly with N in all three regimes as discussed earlier and also decreases slightly with P in regimes I and II. For regime III the critical stress decreases more rapidly with P in agreement with the scaling relationship presented earlier.

Figure 6 shows a plot of the critical slip velocity versus surface coverage for two values of N at constant P. For $\sigma \leqslant \sigma_c$ the critical slip velocity is constant; after σ_c it increases with the surface coverage until $\sigma \sim \sigma_o$. The increase in slip velocity is prominently seen for $N = 18$ (for which $\sigma_c = 0.000\,47$ and $\sigma_o = 0.007$). This increase in critical slip velocity is due to the cooperative decrease in the CR time scale with surface coverage in regime II. However, for $N = 7$ the governing arm retraction process is independent of the surface coverage so the critical slip velocity does not increase in regime II. Above σ_o for $N = 18$ the critical slip velocity remains constant since τ_{CR} is independent of the surface coverage in regime III [see Eq. (19)]. On the other hand, for $N = 7$, the reduced entanglements with bulk chains only helps in faster randomization and hence the critical slip velocity increases with the surface coverage.

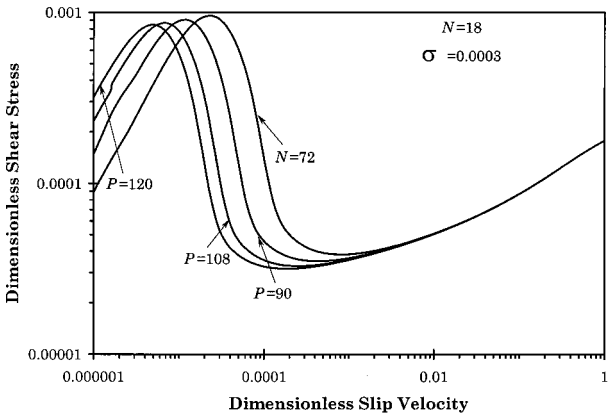

(a)

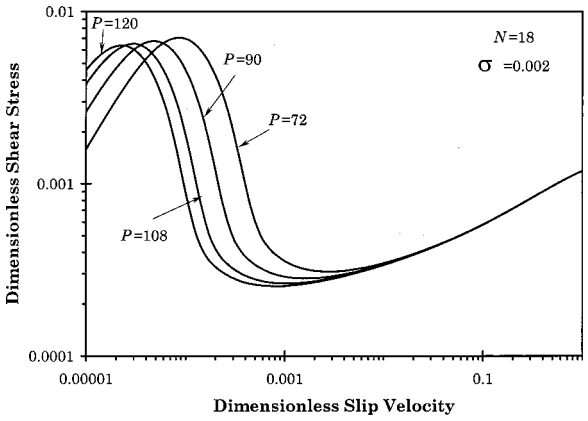

(b)

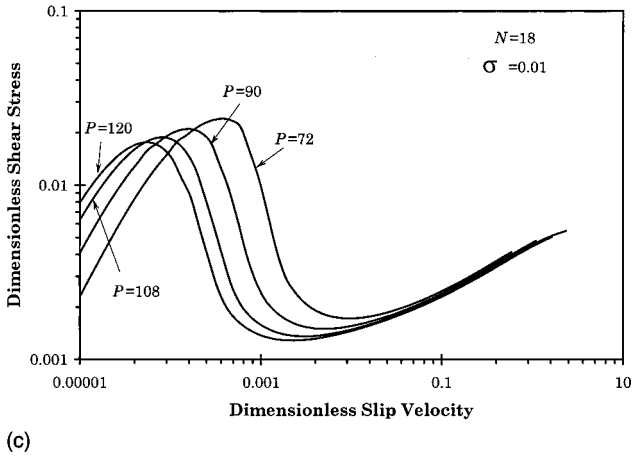

(c)

FIG. 4. Flow curves for tethered chains of chain length $N = 18$ entangled with bulk chains of varying chain lengths: (a) mushroom regime, (b) cooperative regime and (c) overlap regime. The slip velocity was nondimensionalized by the reptation time and the equilibrium contour length of the free chain with 18 segments.

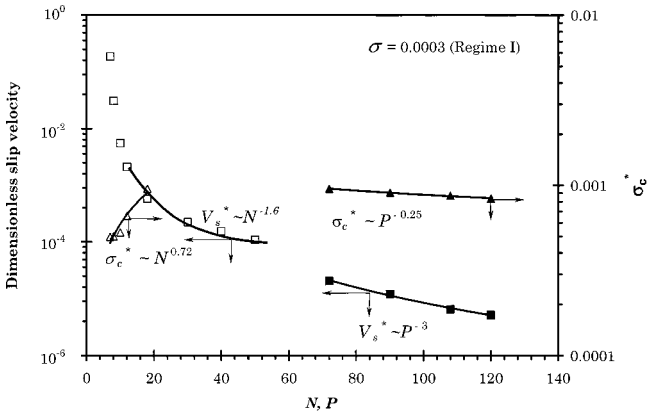

(a)

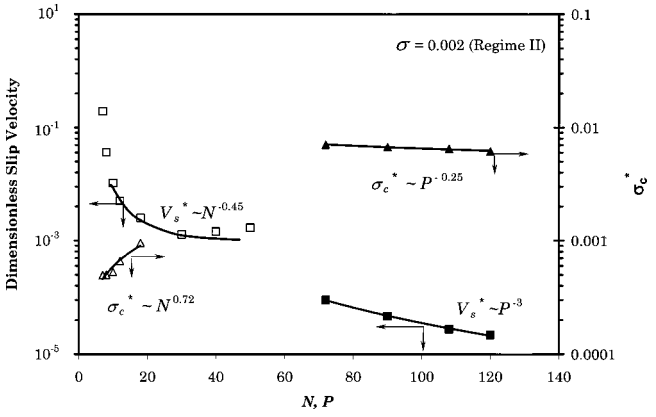

(b)

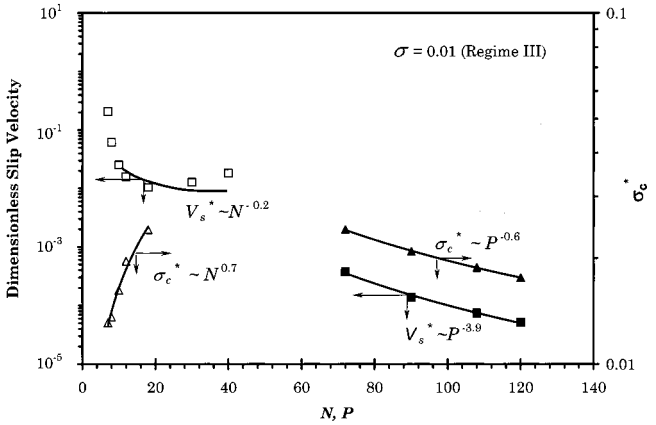

(c)

FIG. 5. Scaling relations for critical slip velocity and critical shear stress calculated by solving the full set of constitutive equations: (a) mushroom regime, (b) cooperative regime and (c) overlap regime. Open symbols represent the data from Fig. 3, and closed symbols represent the data from Fig. 4.

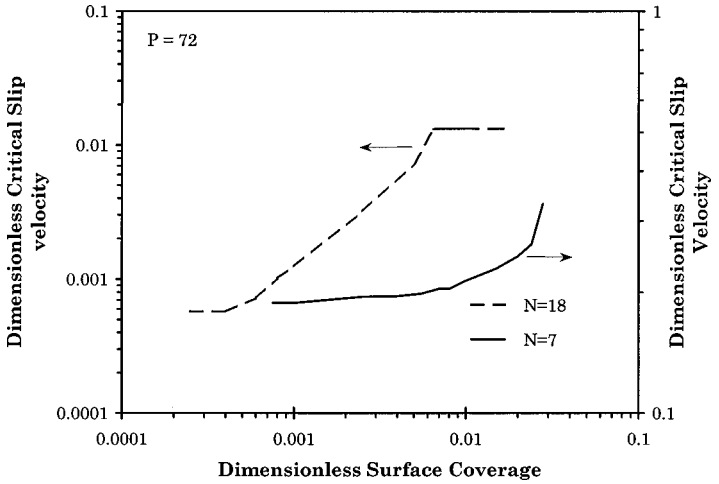

FIG. 6. Critical slip velocity as a function of the dimensionless surface coverage for a short tethered chain ($N = 7$) and a long tethered chain ($N = 18$).

D. Comparison with experimental data

We will now attempt to compare our model predictions with the experimental data of Leger and co-workers [Durliat *et al.* (1997); Leger *et al.* (1999)] on a PDMS melt, which are the only available microscopic experimental data on slip in which the surface is tailored to give end-grafted chains of known molecular weight. The experiments were done using a simple shear apparatus in which the sample was sheared between two flat plates 8 μm apart by moving the top plate at a velocity V_t while maintaining the bottom plate at rest and by measuring the slip velocity near the bottom plate using a novel optical technique. As mentioned earlier, the model parameters are $P, N, \tau_d(P), G^0_{N,B}$ and Σ. Of these, the value of the bulk plateau modulus depends on molecular parameters such as the entanglement molecular weight and the size of the monomer. The estimation of M_e and a' is not unambiguous and hence different experimental techniques would result in different estimates of the value of $G^0_{N,B}$. In this work all information related to the molecular structure has been taken from the work of Fetters *et al.* (1994). Thus the molecular weight between entanglements M_e is estimated to be 13 522 kg/kgmol, the segment length between entanglements is $a = 7.855$ nm and the value of the plateau modulus of the PDMS melt is estimated to be 0.18 MPa [Fetters *et al.* (1994)]. The value of the interfacial modulus can be estimated using Eq. (41). Experimental data are available for a system in which a melt of molecular weight of 970 000 g/gmol ($P = 72$) slides over a layer of end-tethered chains of molecular weight of 96 000 g/gmol ($N = 7$) that has a dimensionless surface coverage in the range of 0.0055–0.03. This range of surface coverage spans regimes II and III (see Fig. 1). Since steady shear rheology data for the bulk polymer were not available, we have estimated its zero shear viscosity from that of a 324 528 g/gmol PDMS melt, which has $\eta_{0,B} = 2000$ Pa s [Leger *et al.* (1996a)]. Thus, the zero shear viscosity of the 970 000 g/gmol melt was estimated to be 63 000 Pa s, from which the reptation time can be estimated to be 0.43 s [$\tau_d(P) = (12/\pi^2)\,\eta_0/G^0_{N,B}$].

Figure 7 shows a comparison between model predictions and the experimental data of slip velocity versus top plate velocity for $\sigma = 0.0055$. Both velocities have been nondimensionalized using the reptation time and the contour length of the bulk chains. The model predicts the qualitative features of the experimental data in that there is a nonzero

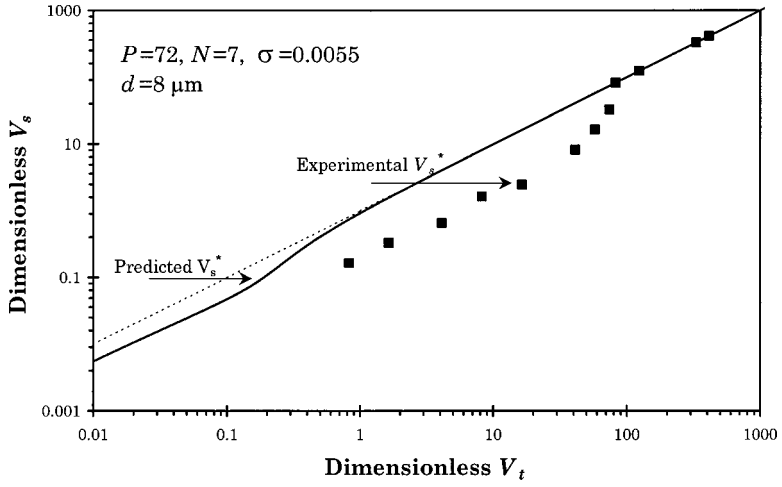

FIG. 7. Comparison of the model prediction with experimental data for the slip velocity of bulk chains near a wall vs the top plate velocity in a simple shear flow apparatus. The experimental data are those of Durliat *et al.* (1997) and of Leger *et al.* (1999).

slip velocity even at small top plate velocities and at a critical top plate velocity the slip velocity rapidly increases and approaches the top plate velocity. The model, however, underpredicts the critical slip velocity as well as the critical top plate velocity at which the jump occurs. For the short tethered chains used in the experiments ($N = 7$) the slip velocity in the low shear region is dictated by the arm retraction process. The higher experimental critical slip velocity value would indicate that the actual relaxation time of the tethered chains is smaller than the calculated arm retractor time. The source of this discrepancy lies probably in the approximate nature of Eq. (14) and/or inaccuracy of the parameters used in it. For example, the reptation time of the N chain was estimated from the reptation time of the bulk chain, which itself is an estimated value. It is also possible that Eq. (14), which considers the arm retraction in a ''fixed tube,'' overestimates the retraction time. Effects such as dynamic dilution [Ball and McLeish (1989)] might provide a realistic prediction of the arm retraction time that will then better predict the experimental critical slip velocity. Underprediction of the critical top plate velocity is due to underprediction of the critical bulk shear rate, which implies that the ratio $G^0_{N,I}/G^0_{N,B}$ calculated by counting the number of entanglements in the interfacial region is smaller than the actual value under experimental conditions.

In Fig. 8 the critical (bulk) shear rate is plotted versus surface coverage. The predicted critical shear rate increases linearly with the surface coverage below overlap coverage σ_o above which it starts decreasing with an increase in surface coverage. As shown in Fig. 2 the interfacial modulus decreases above σ_o and this results in a corresponding decrease in the critical shear stress and hence in the critical shear rate. The experimental data also show an increase in the critical shear rate below σ_o followed by a decrease. Thus, the model correctly predicts the qualitative features of the experimental data. The model also accurately predicts the magnitude of the overlap surface coverage. However, the magnitude of the critical shear rate itself is significantly underpredicted due to underprediction of $G^0_{N,I}/G^0_{N,B}$.

Figure 9 shows a plot of the low shear slip length (b_0) versus surface coverage. The experimental data show that b_0 remains unaffected by the surface coverage. The model predicts a decrease in b_0 with surface coverage below the overlap surface coverage σ_o

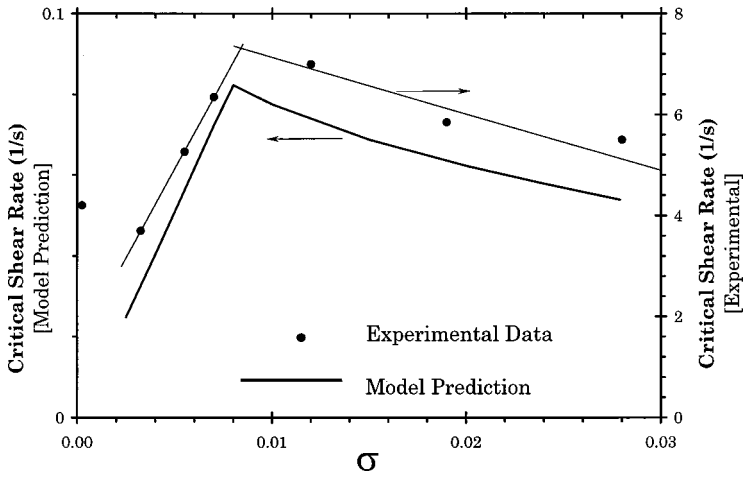

FIG. 8. Predicted critical shear rate as a function of the dimensionless surface coverage for PDMS of $P = 72$ flowing on a wall of end-tethered chains of $N = 7$. The experimental data of Durliat *et al.* (1997) are shown for comparison.

and a nearly constant b_0 after σ_o. At high surface coverage the predicted b_0 is seen to be nearly in quantitative agreement with the experimental data. However, this agreement is fortuitous given the fact that the slip length is the ratio of the slip velocity and shear rate so that errors in the predictions of the numerator and denominator cancel out.

Durliat *et al.* (1997) have further reported that in regimes I and II the critical shear rate scales with the molecular weight of bulk chain as $\dot{\gamma}^* \propto M_{\text{bulk}}^{-3.1\pm0.5}$. In Fig. 10, we plot the critical shear rate and low shear slip length versus the number of segments in the bulk chain at three values of surface coverage, which correspond to regimes I, II, and III. As shown in Fig. 10, the model predicts a strong decrease in the critical shear rate with an increase in P. The power law regression obtained from the model predictions are in agreement with the scaling exponents derived in Sec. III A and are also in agreement with

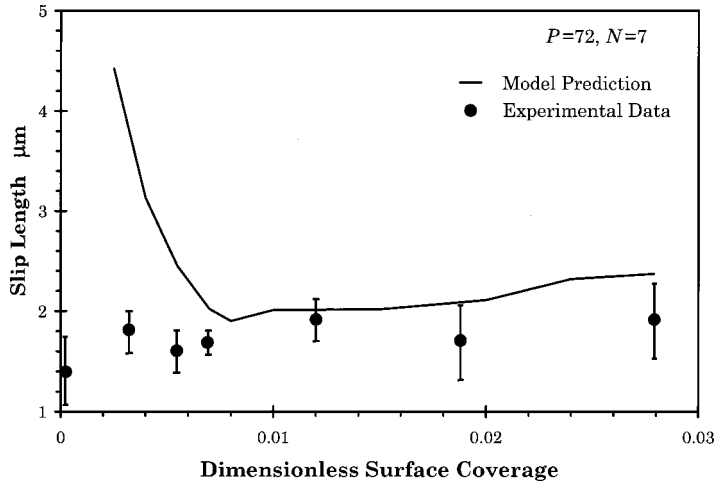

FIG. 9. Comparison of the predicted slip length vs the experimentally determined slip length for various surface coverage values (PDMS of $P = 72$ flowing on a wall of end-tethered chains of $N = 7$).

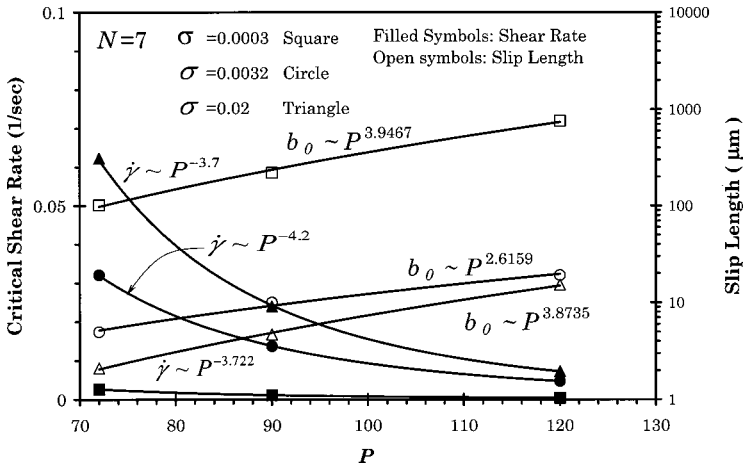

FIG. 10. Scaling laws for critical shear rate and critical slip length for PDMS of different molecular weights flowing on a wall of end-tethered chains of $N = 7$. The critical shear rate is nondimensionalized using the reptation time of the chain with $P = 72$, while the slip length is nondimensionalized using an equilibrium segmental contour length of the chain with $P = 72$.

the scaling reported by Durliat *et al.* (1997). The low shear slip length is predicted to increase with the bulk molecular weight with roughly the same scaling relationships as those derived in Sec. III A. However, this result is in apparent disagreement with the experimental observation of Durliat *et al.* (1997), who observed a bulk molecular weight independent slip length. The scaling laws presented earlier indeed show that the low shear slip length is independent of the bulk molecular weight [see Eqs. (44) and (48)] if the governing relaxation mode were to be CR. However, for short chains such as the ones used in the experiments of Durliat *et al.* (1997) we expect that arm retraction will govern the onset of strong slip. Hence, our model predicts a slip length that is strongly dependent on the bulk molecular weight.

The above discussions show that, while the model predicts many of the experimental data qualitatively, quantitative predictions that are very accurate are not yet possible. It can be noted that errors in the estimation of model parameters will directly affect model predictions of the slip parameters. For instance, the critical stress scales directly as the plateau modulus of the interfacial region and so an error in $G^0_{N,I}$ will translate into a proportional error in the critical stress prediction. Similarly, any errors in the estimation of time scales $\tau_{\mathrm{CR}}, \tau_{\mathrm{AR}}$, and τ_d will result in inaccurate predictions of the slip velocity, critical shear rate, and slip length.

We now attempt to predict the slip data obtained from a *macroscopic* capillary extrusion experiment like those reported by Wang and Drda (1996) and by Yang *et al.* (1998). The apparent wall shear rate in a steady state capillary flow is given by

$$\dot{\gamma}_{w,a} = \frac{4Q}{\pi R^3} = \frac{4}{\sigma^3_{12,w}} \int_0^{\sigma_{12,w}} \dot{\gamma}_b \sigma^2_{12} d\sigma_{12} + 4\frac{(V_s)_{\mathrm{at}\sigma_{12,w}}}{R}. \tag{54}$$

The first term in Eq. (54) represents the contribution from the bulk while the second term is from the boundary condition. Within the context of our model the integral in the first term can be solved by using Eqs. (20)–(25) for a given value of wall shear stress, while the slip velocity is calculated using Eqs. (26)–(34) at the same value of σ_w. Figure 11

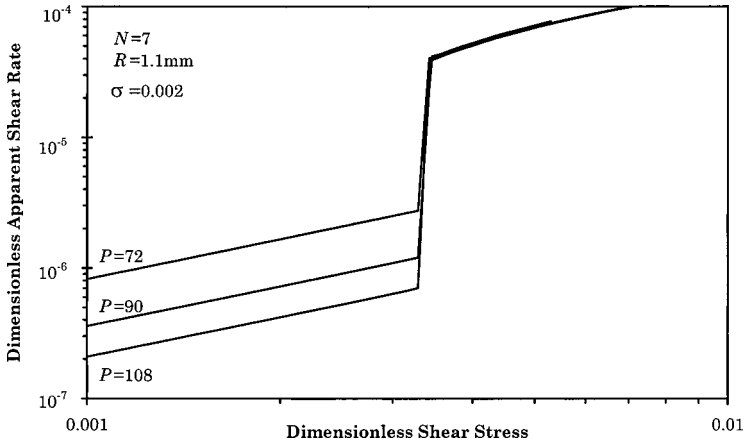

FIG. 11. Prediction of flow curves obtained from controlled stress capillary extrusion of PDMS with molecular weights equivalent to $P = 72$, 90 and 108. The capillary is assumed to have end-tethered PDMS chains of $N = 7$ attached so as to give a dimensionless surface coverage of $\sigma = 0.002$ (regime II). The apparent shear rate was nondimensionalized using the reptation time of a chain with seven segments.

shows calculations of model flow curves in a capillary of 1.1 mm diameter for PDMS melt with chain lengths given by $P = 72$, 90 and 108 at a dimensionless surface coverage (σ) = 0.002 (regime II) and for $N = 7$. The apparent wall shear rate is nondimensionalized by the reptation time of free N chains while the wall shear stress is nondimensionalized by the bulk plateau modulus. The qualitative features of Fig. 11 resemble the capillary extrusion data of Yang *et al.* (1998) remarkably well. First, the capillary flow curve shows a jump discontinuity in the apparent shear rate at critical shear stress. Given that the bulk flow curve is monotonic, it is clear that the strong nonmonotonic nature of the flow curve of tethered chains is directly responsible for the jump discontinuity. Second, the magnitude of the jump discontinuity decreases with a decrease in the bulk molecular weight. Third, the critical stress is independent of the molecular weight and the flow curves on the high slip branch overlap. As far as we know, this is the first time that the full flow curve of a controlled stress capillary extrusion experiment has been predicted using a molecular constitutive equation in which the bulk polymer does not show a nonmonotonic flow curve.

Further, the experimental data on a narrow MWD 1,4-polybutadiene melt shows that the critical stress is independent of the weight averaged molecular weight, which is similar to regime I or II type of behavior. Yang *et al.* (1998) have also reported that the slip length for 1,4-polybutadiene *after a strong slip* is given by $b \sim M_w^{3.5}$. Indeed, Eq. (38) suggests that if $\sigma_{12,I}^*$ and V_s after strong slip were independent of P, then $b \sim \eta_{0,B} \sim P^{3.4}$. $\sigma_{12,I}^*$ is clearly independent of P; similarly, V_s after strong slip is expected to be independent of P because the molecular relaxation along the high slip branch is governed by segmental relaxations (such as contour length fluctuations) rather than by the entire contour length. Thus, the predicted scaling relationship for slip length after strong slip also agrees with their experimental data. Finally, their experimental data for polybutadiene shows that the critical shear rate scales as $M_w^{-3.5}$, which is also in agreement with regime I or II type behavior. We wish to caution here that our analysis is valid only for the case of end-tethered chains whereas in the experimental extrusion experiments the wall probably consists of physically adsorbed chains that form an interfacial layer of loops and tails. It is thus remarkable that the model can even qualitatively

predict most of the experimental observations. It is possible that the loops may provide strong adhering junctions while the tails behave as end-tethered chains. However, in order to compare the model in more detail with any macroscopic extrusion data on slip it is first necessary to analyze the case of loops separately.

IV. CONCLUSIONS

In this article, we have proposed a molecular model for the dynamics of end-tethered chains on a highly adhesive wall over a wide range of grafting densities that span the mushroom regime, the cooperative regime and the overlap regime. We assume all possible relaxation modes of tethered chains, namely, constraint release, arm retraction, convective constraint release and contour length fluctuations. The constitutive equation for the tethered chains is coupled with that for the bulk chains through the continuity of the stress boundary condition. Our model can predict the slip velocity and slip length for a given bulk shear rate or wall shear stress. Further, the model can also predict the flow curve obtained in a capillary extrusion experiment using only molecular parameters.

The model for tethered chains predicts a strongly nonmonotonic flow curve, which is due to suppressed convective constraint release relaxation at the wall. This nonmonotonic nature gives rise to the stick–slip transition in the shear flow of entangled melts. We predict that below the overlap surface coverage the interfacial plateau modulus increases with the surface coverage, while above the overlap surface coverage, it decreases with the surface coverage. This is due to the gradual expulsion of bulk chains from the interfacial region at higher surface coverage. The decrease in the interfacial modulus above overlap coverage also results in a decrease in the critical stress and critical (bulk) shear rate for stick/slip. These predictions agree with the experimental observations. In addition, the predicted value of overlap surface coverage is in excellent agreement with the experimental data. Further, the model predicts several scaling relations between the slip variables and experimental control parameters. These approximate relations are in agreement with earlier scaling models and are also in agreement with microscopic and macroscopic experimental data of slip on highly adhesive walls. A complete solution of the constitutive equation shows minor variations from the scaling relations. Most important, the full solution of the model allows a direct comparison with available experimental data. We find that it is essential to have a good estimate for the arm retraction and constraint release relaxation times for the tethered chains in order to correctly predict the experimental critical slip velocity data. Our model seems to severely underpredict the interfacial plateau modulus, the reason for which is not clear at this time.

The model described in this article is a step forward in providing quantitative understanding of the dynamics of tethered chains at various grafting densities. In a real extrusion scenario, the polymer chains near the wall would most likely form loops and tails when adsorbed onto the wall. Further challenges in modeling include understanding of the behavior of adsorbed loops and of adsorbed branched polymers.

APPENDIX

We summarize the procedure followed for solving the set of integrodifferential constitutive equations. The procedure for solving the CV model for bulk chains is similar to that described elsewhere [Mead *et al.* (1998); Marrucci and Grizzuti, (1988); Mead *et al.* (1995); Mead and Leal (1995)]. For any given choice of shear rate $\kappa_{12,B}$, $Q_{12,B}$ is calculated as a function of θ once and for all. After that the following trial-error loop needs to be solved.

(1) Assign some value to $S_{12,B}(s_0)$ and consider $s = s_0$.
(2) Calculate the value of $\langle v_B(s)\rangle$ using Eq. (24).
(3) Integrate Eq. (21) for s using the tridiagonal matrix system.
(4) Now using the corrected value of s go to step (2) and then to step (3) until s converges.
(5) Integrate Eq. (23) to calculate $G_B(s,\theta)$.
(6) Using Eq. (22) calculate $S_{12,B}$, compare it with the value assigned in step (1); if the error is not below the limit allowed, then start from step (1) with the corrected values of $S_{12,B}$. Recycle the loop until $S_{12,B}$ converges.
(7) Using Eq. (20) calculate the shear stress.

The procedure for solving the slip model is similar to that for the CV model except that it is more complicated because of the coupling between the bulk and interfacial regions through stress continuity. Also, the retraction velocity required for CCR relaxation of tethered chains has to be calculated from the constitutive equation of the bulk while simultaneously maintaining the stress continuity between the two regions. For a given value of $\kappa_{12,I}$, the value of shear stress in the interfacial region is initially predicted from Eqs. (26) to (35) assuming $\langle v_2\rangle = 0$. The procedure for this is similar to that for the CV model described earlier. $\langle v_2\rangle$ is then calculated from the bulk constitutive equation at the same shear stress by inverting Eqs. (20)–(26) numerically. Next, this value of $\langle v_2\rangle$ is used to solve the constitutive equation for the interfacial region to predict a new value of the stress. This procedure is repeated until the shear stress and $\langle v_2\rangle$ converge between previous and current iterations. An alternative procedure would be to first choose a value of the bulk shear rate $\kappa_{12,B}$ and calculate $\langle v_2\rangle$ and stress in the bulk using Eqs. (20)–(26). Next, the interfacial shear rate $\kappa_{12,I}$ and, consequently, the slip velocity are calculated by inverting Eqs. (26)–(35) for the same value of pf in the bulk stress. In either procedure numerical inversion of the integrodifferential equations is required so as to calculate the shear rate for a given value of shear stress. This is done by a brute force technique in which the stress is calculated for a range of shear rates and that shear rate which matches the bulk and interfacial stress values is chosen. We find that the numerical scheme is robust up to a high value of the interfacial shear rate ($\kappa_{12,I} > 1/\tau_{R,I}$) after which convergence is seriously affected due to a change in the nature of the equations from parabolic to hyperbolic.

NOMENCLATURE

a = entanglement distance or tube diameter
a' = monomeric length scale
b_0 = slip length before strong slip
D_{eff} = $D_{\text{eff}} = \phi D_I + (1-\phi)D_{\text{AR}} = \phi D_{\text{CR}} + D_{\text{AR}}$
D_I = $D_I = D_{\text{CR}} + D_{\text{AR}}$
D_{AR} = arm retraction diffusivity
D_{CR} = constraint release diffusivity
D_{rep} = reptative or longitudinal diffusivity
$\mathbf{E}$ = deformation or strain tensor
$f(q)$ = switch function
G = segment renewal probability
G_N^0 = plateau modulus
h = thickness of the interfacial region
k = Boltzmann constant, 1.38×10^{-23} J molecule^{-1} K^{-1}

L = contour length of the deformed tube
L_0 = contour length of the tube at an equilibrium or no-flow condition
N = number of segments in the tethered molecule
N' = number of monomers in the tethered molecule
N_e = average number of monomers between two entanglements
P = number of segments in the bulk molecule
P' = number of monomers in the bulk molecule
q = segmental stretch $= ds/ds_0$
R = radius of the capillary
s = contour length variable of the deformed chain
s_0 = contour length variable of the undeformed chain
S_{12} = shear component of the orientational order parameter tensor
T = absolute temperature
V_s = slip velocity
$\langle\ \rangle$ = average over configuration distribution function

Greek letters

χ = average number of entanglements that one bulk chain makes with a tethered chain
ϕ = fraction of the total number of entanglements in the interfacial region that the tethered chains make with the bulk chains
ϕ_T = volume fraction of the tethered chains
$\dot{\gamma}_{w,a}$ = apparent shear rate
$\eta_{0,B}$ = zero shear viscosity
κ_{12} = shear rate
Σ = surface coverage, number of tethered chains per unit area
Σ_P = number of bulk chains near the wall per unit area
σ = dimensionless surface coverage ($\sigma = \Sigma a'^2$)
σ_c = critical surface coverage (separating the mushroom regime and cooperative regime)
σ_o = overlap surface coverage
σ_P = $\Sigma_P a'^2$
$\sigma_{12,w}$ = wall shear stress
σ_{12} = shear stress
τ_{AR} = arm retraction time scale
τ = dominant relaxation time of the entangled system
τ_ξ = fluctuation time scale
τ_{CR} = relaxation time due to constraint release of a tethered molecule
τ_d = reptation time
τ_R = rouse relaxation time or retraction time
v_1 = velocity of the tube (mesh) with respect to the respective segment of the test chain
v_2 = velocity of the chain end of the bulk chain towards its center due to continuous retraction
v = tangential velocity towards the center of the chain, which arises due to continuous retraction
ξ = $(1-2|s(s_0)|/L)$

Subscripts

I = interfacial region containing tethered molecules

B = bulk region (or bulk chains)
CR = constraint release
AR = arm retraction

References

Ajdari, A. F., F. Brochard-Wyart, P. G. de Gennes, L. Leibler, J. L. Viovy, and M. Rubenstein, ''Slippage of an entangled polymer melt on a grafted surface,'' Physica A **204**, 17–39 (1994).

Ball, R. C. and T. C. B. McLeish, ''Dynamic dilution and the viscosity of star-polymer melts,'' Macromolecules **22**, 1911–1913 (1989).

Brochard, F. and P. G. de Gennes, ''Shear-dependent slippage at a polymer/solid interface,'' Langmuir **8**, 3033–3037 (1992).

Brochard-Wyart, F. A., A. Ajdari, L. Leibler, M. Rubinstein, and J. L. Viovy, ''Dynamics of stars and linear chains dissolved in a polymeric melt,'' Macromolecules **27**, 803–808 (1994).

Brochard-Wyart, F., C. Gay, and P. G. de Gennes, ''Slippage of polymer melts on grafted surfaces,'' Macromolecules **29**, 377–382 (1996).

Denn, M. M., ''Extrusion instabilities and wall slip,'' Annu. Rev. Fluid Mech. **33**, 265–287 (2001).

Durliat, E., H. Hervet, and L. Leger, ''Influence of grafting density on wall slip of a polymer melt on a polymer brush,'' Europhys. Lett. **38**, 383–388 (1997).

Fetters, L., D. J. Lohse, D. Richter, T. A. Witten, and A. Zirkel, ''Connection between polymer molecular weight, density, chain dimensions, and melt viscoelastic properties,'' Macromolecules **27**, 4639–4647 (1994).

Graessley, W. W., ''The entanglement concept in polymer rheology,'' Adv. Polym. Sci. **16**, 1–179 (1974).

Joshi, Y. M., ''Studies on wall slip in entangled polymeric liquids,'' Ph.D. thesis, Indian Institute of Technology, Bombay, Mumbai, 2001.

Joshi, Y. M., A. K. Lele, and R. A. Mashelkar, ''Slipping fluids: A unified transient network model,'' J. Non-Newtonian Fluid Mech. **89**, 303–335 (2000a).

Joshi, Y. M., A. K. Lele, and R. A. Mashelkar, ''A unified wall slip model,'' J. Non-Newtonian Fluid Mech. **94**, 135–149 (2000b).

Joshi, Y. M., A. K. Lele, and R. A. Mashelkar, ''A molecular model for wall slip: Role of convective constraint release,'' Macromolecules **34**, 3412–3420 (2001).

Leger, L., H. Hervet, and G. Massey, ''Slip at wall,'' in *Rheology for Polymer Melt Processing*, edited by J.-M. Piau and J.-F. Agassant (Elsevier Science, Amsterdam, 1996b), pp. 337–355.

Leger, L., E. Raphael, and H. Hervet, ''Surface-anchored polymer chains: Their role in adhesion and friction,'' Adv. Polym. Sci. **138**, 185–225 (1999).

Leger, L., H. Hervet, G. Massey, and E. Durliat, ''Wall slip in polymer melts,'' J. Phys.: Condens. Matter **9**, 7719–7740 (1997).

Leger, L., H. Hervet, P. Auroy, E. Boucher and G. Massey, ''The reptation model: Tests through diffusion measurements in linear polymer melts,'' in *Rheology for Polymer Melt Processing*, edited by J.-M. Piau and J.-F. Agassant (Elsevier Science, Amsterdam, 1996a), pp. 1–16.

Marrucci, G. and N. Grizzuti, ''Fast flows of concentrated polymers: Predictions of the tube model on chain stretching,'' Gazz. Chim. Ital. **118**, 179–185 (1988).

Mead, D. W. and L. G. Leal, ''The reptation model with segmental stretch. I. Basic equations and general properties,'' Rheol. Acta **34**, 360–383 (1995).

Mead, D. W., R. G. Larson, and M. Doi, ''A molecular theory for fast flows of entangled polymers,'' Macromolecules **31**, 7895–7914 (1998).

Mead, D. W., D. Yavich, and L. G. Leal, ''The reptation model with segmental stretch. II. Steady flow properties,'' Rheol. Acta **34**, 339–359 (1995).

Mhetar, V. and L. A. Archer, ''Slip in entangled polymer solutions,'' Macromolecules **31**, 6639–6649 (1998).

Wang, S.-Q., ''Molecular transitions and dynamics at polymer/wall interfaces: origins of flow instabilities and wall slip,'' Adv. Polym. Sci. **138**, 227–275 (1999).

Wang, S.-Q. and P. A. Drda, ''Super fluid like stick–slip transition in capillary flow of linear polyethylene melt. 1. General Features,'' Macromolecules **29**, 2627–2632 (1996).

Watanabe, H., ''Viscoelasticity and dynamics of entangled polymers,'' Prog. Polym. Sci. **24**, 1253–1403 (1999).

Yang, X., A. Halasa, H. Ishida, and S. Q. Wang, ''Experimental study of interfacial and constitutive phenomena in fast flow. 1. Interfacial instabilities of monodisperse polybutadiene,'' Rheol. Acta **37**, 415–423 (1998).